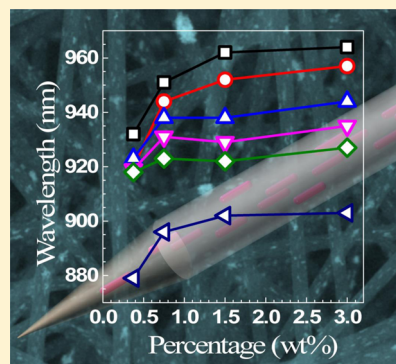


# Manipulating the Collective Surface Plasmon Resonances of Aligned Gold Nanorods in Electrospun Composite Nanofibers

Ying Bao,<sup>†</sup> Hao Fong,<sup>‡</sup> and Chaoyang Jiang<sup>\*,†</sup><sup>†</sup>Department of Chemistry, University of South Dakota, Vermillion, South Dakota 57069, United States<sup>‡</sup>Department of Chemistry, South Dakota School of Mines and Technology, Rapid City, South Dakota 57701, United States**S** Supporting Information

**ABSTRACT:** Surface plasmon resonance (SPR) is an interesting optical property that has been intensively studied in recent years. Herein, we report that the SPRs of gold nanorods (Au NRs) embedded in electrospun poly(vinyl alcohol) nanofibrous films can be manipulated via several approaches such as the change of Au NR percentage in the composite nanofibers, swelling-induced refractive index decrease of local environment, and swelling-induced increase of inter-rod distances among the embedded Au NRs. The electrospun composite nanofibrous films exhibit excellent sensing ability to the swelling solvents with short responsible time and remarkable reversibility. This study advances the fundamental understandings of plasmonic properties for electrospun composite nanofibrous films; thus, it can benefit the novel design of smart nanomaterials for broad sensing and nanophotonic applications.

**INTRODUCTION**

Metallic nanostructures and their composites have attracted growing interest as a typical type of plasmonic nanomaterial due to their unique property of surface plasmon resonances (SPRs).<sup>1–4</sup> The phenomenon of SPR occurs when valence electrons in the metallic nanomaterials can be collectively oscillated upon the stimulation of incident light, and it is responsible for a variety of optical properties including extremely high extinction coefficients, tunable refractive indices, and surface-enhanced Raman scattering (SERS).<sup>5–10</sup> Noble metals, which include gold, silver, and copper, have been extensively investigated for their plasmonic properties via being fabricated into nanostructures. When assembled into organized arrays, these metallic nanostructures would also exhibit additional properties such as superior SERS<sup>11,12</sup> and negative refractive index.<sup>13–16</sup> Consequently, these SPR-active metallic nanostructures have been widely utilized as smart nanomaterials for various applications ranging from single-molecular imaging to ultrasensitive detectors, integrated optical devices, metamaterials, mechanical switching, and photothermal therapy.<sup>17–19</sup> Nevertheless, systematic understandings on the structure–property relationships are still in demand for designing novel plasmonic nanomaterials with improved performances.

The characteristics of SPRs are determined by the size, shape, structure, aggregation, composition, and assembly of metallic nanostructures.<sup>20–24</sup> Furthermore, they are also extremely sensitive to external environment, for example, the surface attachment/bonding of exterior molecules, and the polymer and/or solvent surrounding the plasmonic structures.<sup>25–29</sup> Gold is one of the most studied plasmonic materials.<sup>30–32</sup> Various gold nanostructures, such as nanospheres, nanorods,

nanowires, nanocubes, nanoframes, and nanoshells, have demonstrated their unique SPR modes, which are highly influenced by their nanoscale structures.<sup>22,33–37</sup> Unlike gold nanospheres, gold nanorods (Au NRs) exhibit two SPR modes in the transverse and longitudinal directions due to their one-dimensional morphological structures.<sup>35,38</sup> Both experimental results and theoretical simulations have indicated that the longitudinal SPR (LSPR) mode of Au NRs is substantially more sensitive to environment than the transverse SPR mode. Bao and co-workers recently prepared multilayer thin films (via a layer-by-layer method) containing gold nanoparticles and Au NRs.<sup>39</sup> Their results revealed that the LSPR mode of multilayer thin films of Au NRs could be tuned within a broad range of visible and near-infrared regions.<sup>39</sup> It is noteworthy that the SPRs of nanocomposite materials are more complicated since there are many determining factors from various components of nanocomposites.<sup>40–43</sup> Each of the extinction spectra obtained from experiments is generally an overall result of several factors that can affect the SPRs. Those factors can manipulate the SPR conditions of nanocomposites either synergistically or competitively. Although it is demanding and extremely important, there have been few reports on simultaneous study of two or three factors within nanocomposites due to the lack of suitable systems.

To facilitate their applications, plasmonic nanomaterials have to be carefully designed and integrated into hierarchical nanostructures with large surface areas and easy accessibility for probe analytes. The technique of electrospinning provides a

Received: July 26, 2013

Revised: September 19, 2013

Published: September 23, 2013

convenient and straightforward approach for the preparation of plasmonic nanocomposites.<sup>44</sup> Composite nanofibers with controlled diameters can be readily electrospun with various plasmonic nanomaterials to achieve the desired morphologies and structures.<sup>45–48</sup> The incorporation of Au NRs into electrospun nanofibers has recently been reported with potential applications in optical sensing,<sup>49</sup> surface-enhanced Raman scattering,<sup>45</sup> and polarization-dependent optics.<sup>50</sup> The Au NRs are typically well-aligned in the electrospun composite nanofibers.<sup>46,49–51</sup> Such an alignment of Au NRs in nanofibers, together with the strong interaction between nanorods and polymer matrix, can significantly impact the SPR property of the resulting composite nanofibers. However, there are very few systematic studies on the environmental impacts of the SPR property of Au NRs in composite nanofibers.

In this work, the LSPR shift of Au NRs aligned in electrospun nanofibers was investigated, and the optical property was revealed to be strongly impacted by several parameters simultaneously and competitively. More specifically, poly(vinyl alcohol) (PVA) nanofibrous films containing Au NRs were prepared via electrospinning. The LSPR shifts of Au NRs in the nanofibers were systematically studied when a series of organic solvents were utilized to swell the nanofibrous films. Additionally, the extinction spectra of aligned Au NRs in various matrices were simulated using the method of finite-difference time-domain (FDTD) analyses. Both experimental data and theoretical calculations demonstrated a unique LSPR sensing mechanism in the well-designed composite nanofibers. Critical comparisons were made on several important factors which impacted the LSPR behaviors of the composite nanofibers. This work advanced our fundamental understandings on the plasmonic properties of composite nanofibers, thus allowing the fabrication of novel smart electrospun nanomaterials for applications such as metamaterials and sensing devices.

## ■ EXPERIMENTAL METHODS

**Synthesis of Au NRs.** The Au NRs were synthesized via a well-known seed-mediated growth method using cetyltrimethylammonium bromide (CTAB) as the surfactant.<sup>52</sup> In a typical synthesis, a solution was first prepared by adding HAuCl<sub>4</sub> (0.01 M, 0.25 mL) into CTAB (0.1 M, 10 mL) with gentle mixing. Subsequently, a freshly prepared, ice-cold NaBH<sub>4</sub> solution (0.01 M, 0.6 mL) was quickly injected into the solution followed by being vigorously stirred for 2 min. The obtained seed solution was then ready for further use after being kept at room temperature for 2 h. The growth solution was prepared in a 50 mL plastic tube by mixing CTAB (0.1 M, 40 mL) with HAuCl<sub>4</sub> (0.01 M, 2.0 mL), AgNO<sub>3</sub> (0.01 M, 0.4 mL), HCl (1.0 M, 0.8 mL), and L-ascorbic acid (0.1 M, 0.32 mL). Finally, the seed solution (0.096 mL) was rapidly added into the growth solution. The resulting solution was stirred gently for 10 s and then left undisturbed overnight. The as-synthesized Au NRs were purified by centrifugation for further use.

**Preparation of Electrospun Nanofibers.** The synthesized Au NRs were dispersed in 7 wt % PVA aqueous solution with the desired ratios of polymer versus gold. The concentrations of Au NRs were 3 wt % or lower in the spin dopes. During the electrospinning process, the spin dopes were respectively filled into a 12 mL syringe attached with an 18 gauge metal needle, and a high voltage of 15 kV was applied to the needle. An electrically grounded metal plate covered with

aluminum foil was placed at 12 cm away from the needle as the nanofiber collector. A solution feed rate of 0.6 mL/h was maintained using a KDS200 syringe pump purchased from the KD Scientific Inc. (Holliston, MA). The thickness of electrospun composite nanofibers (consisting of Au NRs impregnated in PVA) was controlled by the electrospinning time, which was typically around 30 min.

**Characterization and Simulation.** The prepared electrospun composite nanofibers containing Au NRs were characterized in terms of their morphological, compositional, structural, and optical properties. Microstructures and morphologies of the nanofibrous films were examined using a JEOL 6700 field-emission scanning electron microscope (SEM). Additional studies on the nanostructures were conducted on a transmission electron microscope (TEM, Tecnai Spirit G2 Twin, FEI Company) operated at the voltage of 120 kV. The SPR of Au NRs was investigated by measuring the extinction spectra of Au NRs in aqueous solutions and organic solutions and in the nanofibrous films. The extinction spectra were measured with a Cary 50 UV–vis spectrophotometer, and the corresponding solvents/substrates were used as blanks in the experiments. PVA-based composite nanofibers could be swollen in various organic solvents, and such swelling might affect the aggregation of Au NRs. The nanofibrous films (attached to glass substrates) were immersed in a cuvette with organic solvents, and the UV–vis extinction spectra were recorded for analyses. The extinction spectra were also calculated with a finite-difference time-domain method using the EM Explorer software. Au NRs with the size of 19 × 72 nm were constructed in the software for electromagnetic field simulations. The optical parameters (*n* and *k*) of gold were obtained from the SOPRA N&K Database. A 512 nm grid size and 2.0 nm Yee cell were used in the spectral simulation. To study the SPR dependence on the inter-rod distance, two Au NRs were constructed in the simulation space, and their inter-rod distance was manually manipulated.

## ■ RESULTS AND DISCUSSION

**Morphology and Composition of Au NR Nanofibrous Films.** The thin films of composite nanofibers containing Au NRs were electrospun from uniform aqueous mixtures of PVA and Au NRs. The Au NRs had the average length and diameter of 71.9 ± 8.7 nm and 18.6 ± 3.4 nm, respectively. The sizes of Au NRs are larger than those of nanorods obtained using classical seed-mediated methods (for example: approximately 45 × 15 nm).<sup>50,53,54</sup> This is quite reasonable since the size and aspect ratio of gold nanorods are extremely sensitive to the experimental conditions, and a slight adjustment in the receipt can produce different nanorods.<sup>49,55–58</sup> The color of aqueous mixture was brown when the concentrations of Au NRs were relatively high (Figure S1, Supporting Information), and the mixture exhibited two extinction peaks around 514 and 826 nm in the UV–vis spectrum (Figure 1a). These two peaks could be attributed to the SPR modes at transverse and longitudinal directions, respectively. After being electrospun into composite nanofibers, the Au NRs still possessed the characteristic optical property, and the composite nanofibrous films turned dark purple. Both transverse and longitudinal SPR modes of Au NRs appeared in the UV–vis spectrum of the nanofibrous film. Compared to the spectrum of aqueous mixture, the transverse peak emerged at the similar wavelength while the longitudinal one exhibited a clear red-shift to ~950 nm (Figure 1b). Such a red-shift of LSPR in composite nanofibers was probably due to

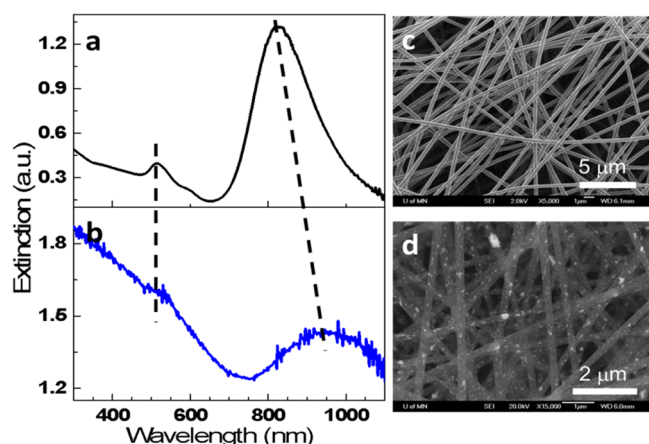


**Figure 1.** UV-vis spectra and SEM micrographs of Au NRs and electrospun composite nanofibers: (a) extinction spectrum of aqueous mixture containing Au NRs; (b) extinction spectrum of composite nanofibrous film electrospun with a solution containing 3.0 wt % Au NR; SEM micrographs of a representative nanofibrous film acquired with low voltage of 2.0 kV (c) and high voltage of 20 kV (d).

the increase of refractive index from 1.333 (water) to 1.519 (PVA).<sup>59</sup> Additionally, the interactions among the Au NRs due to high concentration of Au NRs inside the nanofibers could also be partially responsible for the red-shift. Consistent with previously reported studies, the UV-vis peak of longitudinal

mode appeared to be much more sensitive to the environment than that of transverse mode.<sup>59–61</sup>

SEM was employed to study the morphological structures of nanofibrous films and the distribution of Au NRs in the composite nanofibers. As shown in Figure 1c, the composite nanofibers were randomly overlaid on aluminum foils, and the diameters of these nanofibers were quite uniform ( $229 \pm 18$  nm). The smooth surface of composite nanofibers indicated that the Au NRs might have completely impregnated inside the nanofibers. The inside Au NRs are invisible in SEM images taken at low acceleration voltage (2.0 kV in our case), since the low-energy electrons have much shorter penetration depths in the PVA polymer. On the other hand, the SEM images taken under high voltage (20 kV) are quite different. As shown in Figure 1d, the nanofibers became semitransparent, and the embedded Au NRs were clearly identifiable for orientation, density, and aggregation. We found that both isolated and aggregated Au NRs were presented in the nanofibers. The nanorods were much brighter than the polymer matrix in the SEM images because of the stronger electron scattering by gold atoms. Collectively, valuable morphological and compositional information was obtained on the composite nanofibrous thin films by studying the SEM micrographs taken at both low and high voltages.

Variations of the percentage/amount of Au NRs in the composite nanofibers would result in different colors of nanofibrous films. The percentage controls of Au NRs were achieved by adjusting the concentration of Au NRs in spin

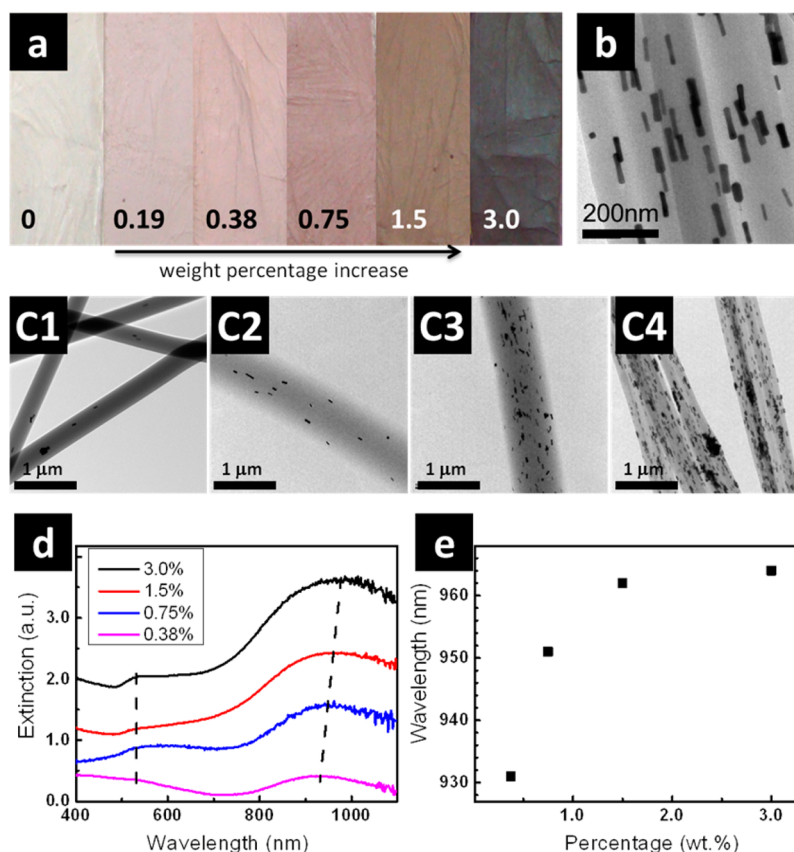


**Figure 2.** (a) Photographs of electrospun composite nanofibrous films containing varied percentages of Au NRs. (b) TEM image showing the aligned Au NR in nanofibers with the Au NRs of 3.0 wt %. (c1–c4) TEM images of electrospun composite nanofibers with Au NR percentages at 0.047, 0.19, 1.5, and 3.0 wt %, respectively. (d) UV-vis extinction spectra of composite nanofibrous films with various percentages of Au NRs in acetone. (e) Summary of LSPR change in acetone as a function of Au NR percentage.

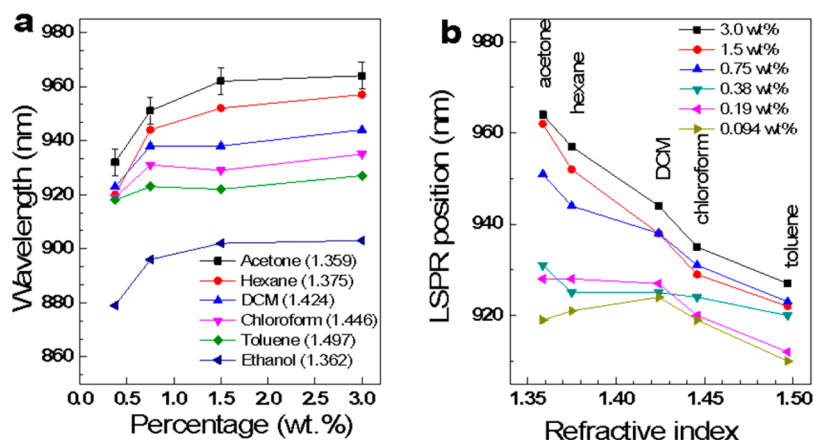


**Figure 3.** UV–vis extinction spectra of composite nanofibrous films with various percentages of Au NRs immersed in different solvents: (a) wavelength of LSPR peaks versus percentage of Au NRs in nanofibrous films; (b) LSPR position versus refractive index of solvent.

dopes. With the increase of Au NR percentage, the color of electrospun nanofibrous films changed from light pink to dark pink then to pinkish blue (Figure 2a). While the intensity of pink color could be simply correlated to the percentage of Au NRs in the nanofibers, the color change from pink to blue was originated from the collective SPR couplings of Au NRs at high loading amounts.

A detail morphological study on the Au NRs embedded in the nanofibers was carried out with a transmission electron microscope (TEM). Figure 2b shows a typical TEM image of electrospun nanofibers with the Au NR weight percentage at 3.0%. It is evident that the Au NRs were aligned in the nanofibers with their long axes parallel to the nanofiber axes. Such an orientation of anisotropic nanomaterials in electrospun nanofibers has been reported by several groups.<sup>50,51,62</sup> This is because anisotropic nanomaterials (e.g., Au NRs) would be oriented during the electrospinning process (particularly during the phenomenon of bending instability), and the introduced orientation would be retained upon the fast evaporation of solvent(s) and formation of nanofibers. The orientation of Au NRs, which would lead to head-to-tail configuration of Au NRs in the nanofibers, could have significant impacts on optical properties of the composite nanofibers.

In addition to the orientation of Au NRs, TEM results also provided other information on the composite nanofibers. Figure 2c shows typical TEM images acquired from the composite nanofibers with Au NR concentrations of 0.047, 0.19, 1.5, and 3.0 wt %. For a better demonstration, here the backgrounds of polymer nanofiber scattering were removed by using pure polymer nanofibrous films as reference samples during the UV–vis measurements. Despite the variance in diameter of the nanofibers which ranged from 220 to 360 nm, these four TEM images showed that the nanofibers had smooth surfaces and the Au NRs were fully embedded inside the fibers. Although TEM images are the projections of the three-dimensional distributions of Au NRs, we can still propose the assembly of Au NRs in a head-to-tail manner, based on the focus-plane observation during the TEM imaging. Furthermore, these TEM micrographs also revealed the amount difference of Au NRs in the nanofibers, suggesting that the weight/volume percentages of Au NRs in electrospun composite nanofibers could be adjusted and controlled.

**Collective SPR Studies.** UV–vis extinction spectra also depicted rational features that were related to environment-

impacted SPRs of the Au NRs. To better analyze the SPR peaks, scattering of polymer nanofibers was largely eliminated by using PVA electrospun nanofibrous films as the blank samples during measurements of UV–vis spectra. As shown in Figure 2d, two characteristic extinction peaks were observed around 515 and 960 nm from the composite nanofibrous thin films, regardless of the volume/weight percentages of Au NRs. These two peaks could be assigned to transverse and longitudinal SPR modes, respectively. Here the extinction intensities of Au NRs in various composite nanofibers are not discussed as much since the thickness of these nanofibrous films are significantly different. Regarding the SPR peak positions, a detailed observation revealed that the positions of transverse peaks barely changed, while the peaks of longitudinal SPRs (LSPRs) had the appreciable red-shift (from 932 to 964 nm in Figure 2e) with the increase of Au NR percentages in the electrospun nanofibers. This red-shift of LSPRs could be attributed to the collective SPR coupling increase of Au NRs in the nanofibers, especially from the Au NRs with head-to-tail orientation that was induced during the electrospinning process. Similar red-shifts of LSPR peaks of Au NRs with head-to-tail orientation were also reported by other researchers.<sup>42,63</sup> Additionally, the red-shift of LSPRs (from 950 to 964 nm) was observed when the nanofibrous films were immersed in the acetone. It is noteworthy that during the swelling process the surrounding medium changed from dry polymer (and air) into swollen polymer in organic solvents. While the detailed mechanisms for LSPR shifts are complicated, we believe that such an LSPR shift could be related to the variation of inter-nanorod interaction, change of reflective index, or a combination of these two mechanisms due to the swelling process.

**Swelling-Induced LSPR Shifts.** It is known that polymers can have varied swelling behaviors in different organic solvents. Therefore, it would be interesting to study the manipulability of Au NR LSPRs where the composite nanofibrous films are immersed in various organic solvents. For example, when the composite nanofibrous films were immersed in ethanol, we observed different LSPR responses as compared to immersing the films in acetone. As shown in Figure 3, the LSPR peak was located around 903 nm for the nanofibrous films with a high weight percentage of Au NRs in ethanol; such a wavelength was much lower than the same films in acetone. This could be attributed to the different swelling behaviors of the composite

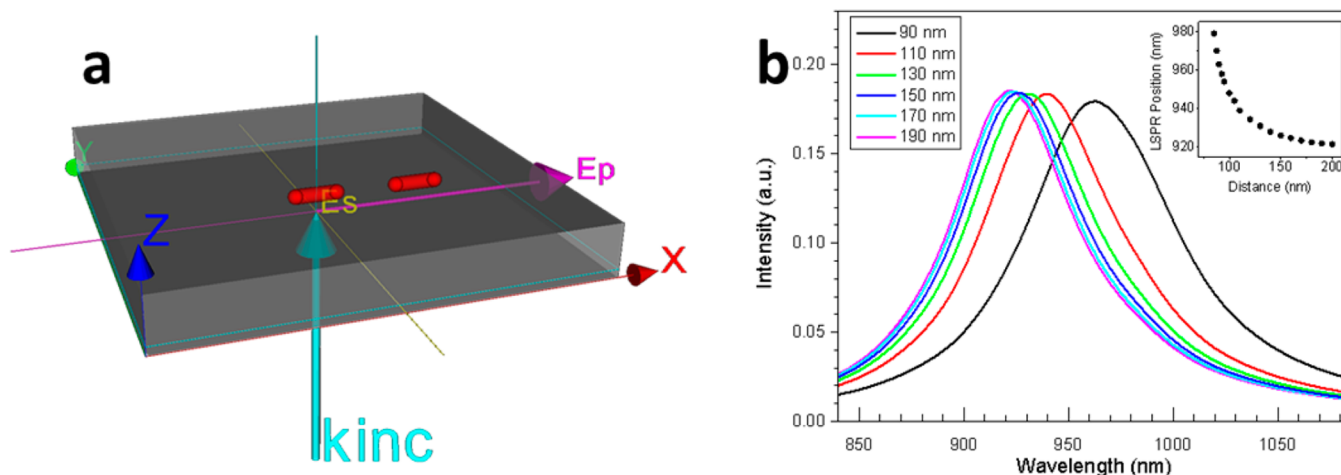


**Figure 4.** (a) A schematic showing that two Au NRs are aligned in a grid with size of  $512 \times 512 \times 64$  nm and their extinction spectra are calculated using a plan wave (p-polarized) as the initial excitation source. (b) Several representative extinction spectra of Au NRs with various inter-rod distances (inset: correlation of the LSPR position with the inter-rod distance).

nanofibers in the two solvents. Ethanol is a better solvent for PVA than acetone; hence, the swelling of composite nanofibers in ethanol would be more significant than that in acetone.<sup>64</sup> Consequently, the degree of orientation for Au NRs inside the nanofibers might be slightly decreased during the polymer swelling, thus reducing the collective LSPR coupling among the nanorods. Such a speculation of swelling-induced orientation reduction was further confirmed by the LSPR shifts for the nanofibrous films with varied Au NR percentages. The positions of those LSPR peaks were essentially unchanged (in the range from 885 to 903 nm), considering the errors of the experimental data. The following is the proposed explanation: owing to the substantial swelling of composite nanofibers in ethanol, the inter-nanorod interactions and collective SPRs are very weak and quite similar, regardless of the percentages of Au NRs in the nanofibers. Therefore, all of these LSPRs appear at similar wavelength, close to those of the composite nanofibers with very low percentage of Au NRs.

Furthermore, the appearance of LSPRs in shorter wavelength might also be partially attributed to the different refractive index (RI) of the surrounding medium when the composite nanofibers were immersed in acetone or ethanol. The RI value of ethanol is 1.362, which is very similar to that of acetone (1.359). However, due to the substantial swelling of composite nanofibers in ethanol, the effective RI value of the surrounding medium near Au NRs would be much lower than that of composite nanofibers in acetone. It is known that the lower RI value in a local environment would result in the blue-shift of LSPRs for Au NRs.

The solvent effect on LSPR modes of Au NRs in composite nanofibers was then studied systematically by using other four organic solvents with different RI values and swelling abilities. Combined with the results from acetone and ethanol, we revealed the correlations among the position of LSPR peaks, percentage of Au NRs, and the RI value of solvents used to immerse the nanofibrous films. The results indicated that the red-shift of LSPR modes would occur upon the increase of Au NR percentages in the composite nanofibers. This was obvious in the cases of acetone, hexane, and dichloromethane (DCM) while less substantial in the cases of chloroform, toluene, and ethanol. The LSPR shifts in varied solvents can be explained with different degrees of swelling of the composite nanofibers.

Strong swelling capabilities of ethanol and toluene to PVA have been well documented in the literature.<sup>65,66</sup> Our results indicated that the swelling of composite nanofibers would become more substantial with the order of acetone, hexane, DCM, chloroform, toluene, and ethanol, and such an order could be related to the polarities and chemical structures of the solvents.

The swelling of composite nanofibers can also significantly change the effective RI of the surrounding medium, thus impacting the LSPR position. Although such an influence can be hardly excluded, the dependence of LSPR positions on the solvent RIs (Figure 3b) gives quite interesting results. Blue-shifts of LSPR peaks were observed for the nanofibrous films with various amounts of the Au NRs. This cannot be rationally explained if only refractive indices of the solvents are considered because, in general, the red-shift of LSPR peaks would be expected upon the increase of refractive indices. Our control experiment clearly demonstrated that the LSPR usually had the red-shift when Au NRs were surface-modified with hexadecanethiol and then directly dispensed in organic solvents (Figure S2a). Such a normal red-shift could also be obtained via the theoretical calculation (Figure S2b). Thus, we believe that for Au NRs in electrospun nanofibers the refractive indices of organic solvents have minor impact on the LSPRs for slightly swollen nanofibers. The experimental results showed that the changes of RI and inter-rod distance would have opposite effects on the LSPR shift. On the basis of the results, it appeared that the change of inter-rod distance would become the dominant factor, and such an explanation would be quite reasonable considering the media surrounding the Au NRs and the significant swelling of the composite nanofibers.

Our speculation on the LSPR shift due to the inter-rod distance changes in composite nanofibers could be further supported by a numerical simulation. Here we applied the FDTD method and calculated the extinction spectra and the LSPR peak position of composite nanofibers under different conditions. Two gold nanorods were aligned in a grid with the size of  $512 \times 512 \times 64$  nm, and their extinction spectra were calculated using a plan wave (p-polarized) as the initial excitation source (Figure 4a). Figure 4b shows several representative extinction spectra of Au NRs with varied inter-rod distances. It is evident that the LSPR peaks are around 920

nm when the two nanorods are far from each other. The decrease of inter-rod distance would result in a red-shift of the LSPRs (inset in Figure 4b). When the two rods are within a distance of 90 nm (center to center), we can obtain a LSPR peak around 960 nm, a value that is similar to the experimental result. Although the theoretical prediction suggests more red-shift for even closer nanorods, it is technically challenging to prepare electrospun composite nanofibers with higher percentages of Au NRs. It is noteworthy that change of the spatial angle and the alignment degree of Au NRs can also contribute to the coupling of Au NRs during the polymer swelling, which requires even detailed experimental designs and investigations. In general, the simulation produces a similar result as the experimental ones, providing further support for our explanation of LSPR blue-shifts using the model of swelling-induced distance increase.

**Fast and Reversible LSPR Sensing.** The swelling-induced inter-rod distance increases result in significant LSPR shifts of electrospun composite nanofibrous films, and these films can be utilized as novel nanostructured materials for solvent sensing. Herein, the LSPR shift sensitivity to organic solvents is originated from the swelling of composite nanofibers, and the swelling then results in the shift of LSPRs of the embedded Au NRs. Compared to dispersing Au NRs in ultrathin films using a drop-casting method, the electrospinning technique is essential for this sensing capability by providing important structural characteristics including unidirectional orientation of Au NRs in the nanofibers. Figure S3 shows the LSPR changes of Au NRs in the electrospun nanofibers and in the cast films. It is evident that the LSPR changes in nanofibers are faster and more significant than those of cast films. The ultrathin fiber diameter allows/facilitates a shorter swelling process for faster sensing. Meanwhile, the alignment of Au NRs leads to the unique head-to-tail nanostructure and makes the LSPR very sensitive to the change of inter-rod distance. It is noteworthy that the initial LSPR positions are not the same for nanofibers and cast films; this might be due to different types of aggregations of Au NRs in these two composite nanostructures, a subject for further systematic investigation.

Excellent reversibility is important for all of the sensing applications. The LSPR shift of Au NRs upon swelling of composite nanofibers was studied by using the solvents of toluene and hexane as external stimulations. The positions of LSPR modes for Au NRs were recorded when the same nanofibrous film was immersed in those two solvents alternatively. As shown in Figure 5, the LSPR positions were around  $959.1 \pm 3.3$  nm when hexane was used for immersion of the nanofibrous films; on the other hand, the same film immersed in toluene showed LSPR positions around  $918.3 \pm 3.1$  nm. In the reversibility tests, the same films could be alternatively immersed in the two solvents for over ten cycles, and the shifts of LSPRs were observed along the change of the organic solvents. Furthermore, the electrospun composite nanofibers containing Au NRs well-retained their morphological structures after these ten cycles. Note that if the neat PVA nanofibers were immersed in ethanol, the fibers would be swollen permanently, and the morphology of fibrous film would no longer exist after immersion. Our results showed that the LSPR modes of Au NRs had a highly reversible sensing behavior upon the selection of swelling solvents. Such results would be critical for the development of novel plasmonic sensing devices for a variety of applications.

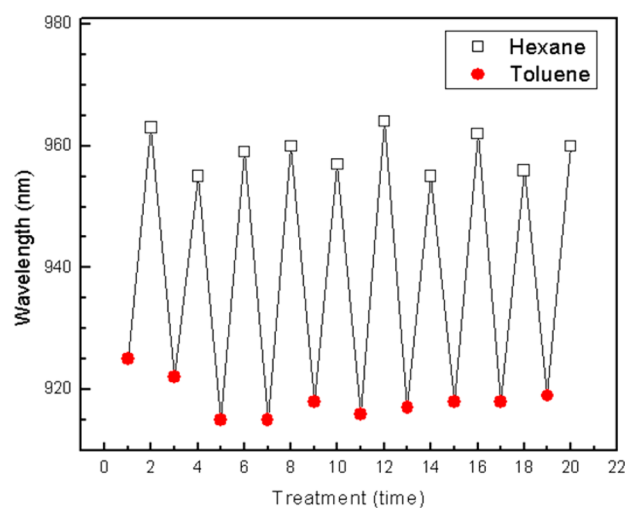


**Figure 5.** Reversibility of LSPR shifts when the electrospun composite nanofibrous films were immersed in toluene and hexane alternatively.

Overall, our results indicate that the swelling-induced increases of inter-rod distances and LSPR shifts of Au NRs embedded electrospun polymeric nanofibers can be ultimately applied in various sensing applications, such as quality evaluations of organic solvents and swelling studies of polymers in organic solvents. To facilitate the quality evaluation of organic solvents, additional structural optimization of the composite nanofibers is necessary to improve the LSPR sensitivity. As for the second possible application of studying the swelling behavior of polymers in various organic solvents, our results have clearly demonstrated that such analyses are capable of being accomplished. More systematic experiments need be conducted to validate and improve such a quantitative technique.

## CONCLUSIONS

In this study, we have demonstrated that the localized surface plasmon resonances of Au NRs embedded in electrospun PVA nanofibrous films can be tuned in the visible and near-infrared regions. Via the immersion of nanofibrous thin films in different organic solvents, the swelling-induced inter-rod distance of Au NRs could be changed, which would significantly affect the LSPR peak positions. Such an impact is much stronger than the change of refractive indices of local environments. Furthermore, the extinction spectra of aligned Au NRs in various matrices were further simulated via the method of finite-difference time-domain analyses. Compared to nanocomposite thin films prepared using the drop-casting method, the electrospun nanofibrous thin films containing Au NRs in head-to-tail orientation can result in interesting coupling behavior and sensing performance. Furthermore, the electrospun nanofibrous films demonstrated much faster sensing due to the sub-micrometer diameters of the nanofibers. The short response time and excellent reversibility were identified for those nanostructured sensing fibrous films. Both experimental data and theoretical calculations provide the improved understanding on the unique plasmonic properties of electrospun composite nanofibers, thus allowing the design and fabrication of novel smart nanostructured materials for broad applications such as plasmonic devices and sensors.

## ■ ASSOCIATED CONTENT

## ● Supporting Information

Photographs of gold nanorod dispersion and nanofibrous films, LSPR peak shift of hydrophobic gold nanorods in various solvents, and LSPR peak shifts of gold nanorods in a fibrous film and a casting film when being swollen in ethanol. This material is available free of charge via the Internet at <http://pubs.acs.org>.

## ■ AUTHOR INFORMATION

## Corresponding Author

\*E-mail [Chaoyang.Jiang@usd.edu](mailto:Chaoyang.Jiang@usd.edu); Fax +1 605 677 6397; Tel +1 605 677 6250 (C.J.).

## Notes

The authors declare no competing financial interest.

## ■ ACKNOWLEDGMENTS

This work was supported by the NSF (Award Numbers EPS-0903804 and DGE-0903685), NASA (Cooperative Agreement Number NNX10AN34A), and the State of South Dakota. Some TEM studies were conducted on the instrument funded by the NSF (Award Number CHE-0840507). SEM studies were carried out in the Characterization Facility at the University of Minnesota, which received partial support from the NSF through the MRSEC program (Award Number DMR-0819885). We thank Drs. James Hoefelmeyer and John Nelson for sample characterizations and valuable discussions.

## ■ REFERENCES

- (1) Willets, K. A.; Van Duyne, R. P. Localized Surface Plasmon Resonance Spectroscopy and Sensing. *Annu. Rev. Phys. Chem.* **2007**, *58*, 267–297.
- (2) Halas, N. J.; Lal, S.; Chang, W.-S.; Link, S.; Nordlander, P. Plasmons in Strongly Coupled Metallic Nanostructures. *Chem. Rev.* **2011**, *111*, 3913–3961.
- (3) Szunerits, S.; Boukherroub, R. Sensing Using Localised Surface Plasmon Resonance Sensors. *Chem. Commun.* **2012**, *48*, 8999–9010.
- (4) Thorkelsson, K.; Nelson, J. H.; Alivisatos, A. P.; Xu, T. End-to-End Alignment of Nanorods in Thin Films. *Nano Lett.* **2013**, DOI: 10.1021/nl402862b.
- (5) Lu, C. H.; Wang, Y. W.; Ye, S. L.; Chen, G. N.; Yang, H. H. Ultrasensitive Detection of  $\text{Cu}^{2+}$  with the Naked Eye and Application in Immunoassays. *NPG Asia Mater.* **2012**, *4*, e10.
- (6) Vilela, D.; Gonzalez, M. C.; Escarpa, A. Sensing Colorimetric Approaches Based on Gold and Silver Nanoparticles Aggregation: Chemical Creativity Behind the Assay. A Review. *Anal. Chim. Acta* **2011**, *751*, 24–43.
- (7) Cai, Z.; Liu, Y. J.; Lu, X.; Teng, J. In Situ “Doping” Inverse Silica Opals with Size-Controllable Gold Nanoparticles for Refractive Index Sensing. *J. Phys. Chem. C* **2013**, *117*, 9440–9445.
- (8) Kodiyath, R.; Malak, S. T.; Combs, Z. A.; Koenig, T.; Mahmoud, M. A.; El-Sayed, M. A.; Tsukruk, V. V. Assemblies of Silver Nanocubes for Highly Sensitive SERS Chemical Vapor Detection. *J. Mater. Chem. A* **2013**, *1*, 2777–2788.
- (9) Rycenga, M.; Cobley, C. M.; Zeng, J.; Li, W.; Moran, C. H.; Zhang, Q.; Qin, D.; Xia, Y. Controlling the Synthesis and Assembly of Silver Nanostructures for Plasmonic Applications. *Chem. Rev.* **2011**, *111*, 3669–3712.
- (10) Kumar, J.; Thomas, K. G. Surface-Enhanced Raman Spectroscopy: Investigations at the Nanorod Edges and Dimer Junctions. *J. Phys. Chem. Lett.* **2011**, *2*, 610–615.
- (11) Gong, X.; Bao, Y.; Qiu, C.; Jiang, C. Individual Nanostructured Materials: Fabrication and Surface-Enhanced Raman Scattering. *Chem. Commun.* **2012**, *48*, 7003–7018.

(12) Gandra, N.; Singamaneni, S. Bilayered Raman-Intense Gold Nanostructures with Hidden Tags (BRIGHTs) for High-Resolution Bioimaging. *Adv. Mater.* **2013**, *25*, 1022–1027.

(13) Kovacs, G. J.; Loutfy, R. O.; Vincett, P. S.; Jennings, C.; Aroca, R. Distance Dependence of SERS Enhancement Factor from Langmuir-Blodgett Monolayers on Metal Island Films: Evidence for the Electromagnetic Mechanism. *Langmuir* **1986**, *2*, 689–694.

(14) Wurtz, G. A.; Pollard, R.; Henden, W.; Wiederrecht, G. P.; Gosztola, D. J.; Podolskiy, V. A.; Zayats, A. V. Designed Ultrafast Optical Nonlinearity in a Plasmonic Nanorod Metamaterial Enhanced by Nonlocality. *Nat. Nanotechnol.* **2011**, *6*, 106–110.

(15) Quan, Z. W.; Fang, J. Y. Superlattices with Non-Spherical Building Blocks. *Nano Today* **2010**, *5*, 390–411.

(16) Guffey, M. J.; Scherer, N. F. All-Optical Patterning of Au Nanoparticles on Surfaces Using Optical Traps. *Nano Lett.* **2010**, *10*, 4302–4308.

(17) Yan, Z.; Shah, R. A.; Chado, G.; Gray, S. K.; Pelton, M.; Scherer, N. F. Guiding Spatial Arrangements of Silver Nanoparticles by Optical Binding Interactions in Shaped Light Fields. *ACS Nano* **2013**, *7*, 1790–1802.

(18) Yoshida, M.; Lahann, J. Smart Nanomaterials. *ACS Nano* **2008**, *2*, 1101–1107.

(19) Gupta, M. K.; Chang, S.; Singamaneni, S.; Drummy, L. F.; Gunawidjaja, R.; Naik, R. R.; Tsukruk, V. V. pH-Triggered SERS via Modulated Plasmonic Coupling in Individual Bimetallic Nanocobs. *Small* **2011**, *7*, 1192–1198.

(20) Gandra, N.; Abbas, A.; Tian, L.; Singamaneni, S. Plasmonic Planet–Satellite Analogues: Hierarchical Self-Assembly of Gold Nanostructures. *Nano Lett.* **2012**, *12*, 2645–2651.

(21) Lu, X.; Tuan, H.-Y.; Chen, J.; Li, Z.-Y.; Korgel, B. A.; Xia, Y. Mechanistic Studies on the Galvanic Replacement Reaction between Multiply Twinned Particles of Ag and  $\text{HAuCl}_4$  in an Organic Medium. *J. Am. Chem. Soc.* **2007**, *129*, 1733–1742.

(22) Chen, H. J.; Shao, L.; Woo, K. C.; Ming, T.; Lin, H. Q.; Wang, J. F. Shape-Dependent Refractive Index Sensitivities of Gold Nanocrystals with the Same Plasmon Resonance Wavelength. *J. Phys. Chem. C* **2009**, *113*, 17691–17697.

(23) Hill, R. T.; Mock, J. J.; Hucknall, A.; Wolter, S. D.; Jokerst, N. M.; Smith, D. R.; Chilkoti, A. Plasmon Ruler with Angstrom Length Resolution. *ACS Nano* **2012**, *6*, 9237–9246.

(24) Campione, S.; Adams, S. M.; Ragan, R.; Capolino, F. Comparison of Electric Field Enhancements: Linear and Triangular Oligomers Versus Hexagonal Arrays of Plasmonic Nanospheres. *Opt. Express* **2013**, *21*, 7957–7973.

(25) Zhang, X.-Y.; Hu, A.; Zhang, T.; Lei, W.; Xue, X.-J.; Zhou, Y.; Duley, W. W. Self-Assembly of Large-Scale and Ultrathin Silver Nanoplate Films with Tunable Plasmon Resonance Properties. *ACS Nano* **2011**, *5*, 9082–9092.

(26) Tagliazucchi, M.; Blaber, M. G.; Schatz, G. C.; Weiss, E. A.; Szeifer, I. Optical Properties of Responsive Hybrid Au@Polymer Nanoparticles. *ACS Nano* **2012**, *6*, 8397–8406.

(27) Davletshin, Y. R.; Lombardi, A.; Cardinal, M. F.; Juve, V.; Crut, A.; Maioli, P.; Liz-Marzan, L. M.; Vallee, F.; Del Fatti, N.; Kumaradas, J. C. A Quantitative Study of the Environmental Effects on the Optical Response of Gold Nanorods. *ACS Nano* **2012**, *6*, 8183–8193.

(28) Mahmoud, M. A.; Chamanzar, M.; Adibi, A.; El-Sayed, M. A. Effect of the Dielectric Constant of the Surrounding Medium and the Substrate on the Surface Plasmon Resonance Spectrum and Sensitivity Factors of Highly Symmetric Systems: Silver Nanocubes. *J. Am. Chem. Soc.* **2012**, *134*, 6434–6442.

(29) Piliarik, M.; Kvasnicka, P.; Galler, N.; Krenn, J. R.; Homola, J. Local Refractive Index Sensitivity of Plasmonic Nanoparticles. *Opt. Express* **2011**, *19*, 9213–9220.

(30) Alvarez-Puebla, R. A.; Agarwal, A.; Manna, P.; Khanal, B. P.; Aldeanueva-Potel, P.; Carbo-Argibay, E.; Pazos-Perez, N.; Vigderman, L.; Zubarev, E. R.; Kotov, N. A.; Liz-Marzan, L. M. Gold Nanorods 3d-Supercrystals as Surface Enhanced Raman Scattering Spectroscopy Substrates for the Rapid Detection of Scrambled Prions. *Proc. Natl. Acad. Sci. U. S. A.* **2011**, *108*, 8157–8161.

- (31) Lohse, S. E.; Murphy, C. J. The Quest for Shape Control: A History of Gold Nanorod Synthesis. *Chem. Mater.* **2013**, *25*, 1250–1261.
- (32) Vigderman, L.; Khanal, B. P.; Zubarev, E. R. Functional Gold Nanorods: Synthesis, Self-Assembly, and Sensing Applications. *Adv. Mater.* **2012**, *24*, 4811–4841.
- (33) Mahmoud, M. A.; El-Sayed, M. A. Gold Nanoframes: Very High Surface Plasmon Fields and Excellent near-Infrared Sensors. *J. Am. Chem. Soc.* **2010**, *132*, 12704–12710.
- (34) Kundu, S.; Lau, S.; Liang, H. Shape-Controlled Catalysis by Cetyltrimethylammonium Bromide Terminated Gold Nanospheres, Nanorods, and Nanoprisms. *J. Phys. Chem. C* **2009**, *113*, 5150–5156.
- (35) Pérez-Juste, J.; Pastoriza-Santos, I.; Liz-Marzán, L. M.; Mulvaney, P. Gold Nanorods: Synthesis, Characterization and Applications. *Coord. Chem. Rev.* **2005**, *249*, 1870–1901.
- (36) Biener, J.; Nyce, G. W.; Hodge, A. M.; Biener, M. M.; Hamza, A. V.; Maier, S. A. Nanoporous Plasmonic Metamaterials. *Adv. Mater.* **2008**, *20*, 1211–1217.
- (37) Lombardi, A.; Loumagne, M.; Crut, A.; Maioli, P.; Del Fatti, N.; Vallée, F.; Spuch-Calvar, M.; Burgin, J.; Majimel, J.; Tréguer-Delapierre, M. Surface Plasmon Resonance Properties of Single Elongated Nano-Objects: Gold Nanobipyramids and Nanorods. *Langmuir* **2012**, *28*, 9027–9033.
- (38) Maity, S.; Kozek, K. A.; Wu, W.-C.; Tracy, J. B.; Bochinski, J. R.; Clarke, L. I. Anisotropic Thermal Processing of Polymer Nanocomposites via the Photothermal Effect of Gold Nanorods. *Part. Part. Syst. Charact.* **2013**, *30*, 193–202.
- (39) Bao, Y.; Vigderman, L.; Zubarev, E. R.; Jiang, C. Robust Multilayer Thin Films Containing Cationic Thiol-Functionalized Gold Nanorods for Tunable Plasmonic Properties. *Langmuir* **2012**, *28*, 923–930.
- (40) Khatua, S.; Manna, P.; Chang, W.-S.; Tcherniak, A.; Friedlander, E.; Zubarev, E. R.; Link, S. Plasmonic Nanoparticles-Liquid Crystal Composites. *J. Phys. Chem. C* **2010**, *114*, 7251–7257.
- (41) Solis, D.; Chang, W.-S.; Khanal, B. P.; Bao, K.; Nordlander, P.; Zubarev, E. R.; Link, S. Bleach-Imaged Plasmon Propagation (BLIPP) in Single Gold Nanowires. *Nano Lett.* **2010**, *10*, 3482–3485.
- (42) Li, W.; Zhang, P.; Dai, M.; He, J.; Babu, T.; Xu, Y.-L.; Deng, R.; Liang, R.; Lu, M.-H.; Nie, Z.; Zhu, J. Ordering of Gold Nanorods in Confined Spaces by Directed Assembly. *Macromolecules* **2013**, *46*, 2241–2248.
- (43) Rodríguez-Fernández, J.; Fedoruk, M.; Hrelescu, C.; Lutich, A. A.; Feldmann, J. Triggering the Volume Phase Transition of Core-Shell Au Nanorod–Microgel Nanocomposites with Light. *Nanotechnology* **2011**, *22*, 245708.
- (44) Greiner, A.; Wendorff, J. H. Electrospinning: A Fascinating Method for the Preparation of Ultrathin Fibers. *Angew. Chem., Int. Ed.* **2007**, *46*, 5670–5703.
- (45) Zhang, C.-L.; Lv, K.-P.; Cong, H.-P.; Yu, S.-H. Controlled Assemblies of Gold Nanorods in PVA Nanofiber Matrix as Flexible Free-Standing SERS Substrates by Electrospinning. *Small* **2012**, *8*, 648–653.
- (46) He, D.; Hu, B.; Yao, Q.-F.; Wang, K.; Yu, S.-H. Large-Scale Synthesis of Flexible Free-Standing SERS Substrates with High Sensitivity: Electrospun PVA Nanofibers Embedded with Controlled Alignment of Silver Nanoparticles. *ACS Nano* **2009**, *3*, 3993–4002.
- (47) Zhang, L.; Gong, X.; Bao, Y.; Zhao, Y.; Xi, M.; Jiang, C.; Fong, H. Electrospun Nanofibrous Membranes Surface-Decorated with Silver Nanoparticles as Flexible and Active/Sensitive Substrates for Surface-Enhanced Raman Scattering. *Langmuir* **2012**, *28*, 14433–14440.
- (48) Bao, Y.; Lai, C.; Zhu, Z.; Fong, H.; Jiang, C. SERS-Active Silver Nanoparticles on Electrospun Nanofibers Facilitated via Oxygen Plasma Etching. *RSC Adv.* **2013**, *3*, 8998–9004.
- (49) Wang, P.; Zhang, L.; Xia, Y. N.; Tong, L. M.; Xu, X.; Ying, Y. B. Polymer Nanofibers Embedded with Aligned Gold Nanorods: A New Platform for Plasmonic Studies and Optical Sensing. *Nano Lett.* **2012**, *12*, 3145–3150.
- (50) Roskov, K. E.; Kozek, K. A.; Wu, W.-C.; Chhetri, R. K.; Oldenburg, A. L.; Spontak, R. J.; Tracy, J. B. Long-Range Alignment of Gold Nanorods in Electrospun Polymer Nano/Microfibers. *Langmuir* **2011**, *27*, 13965–13969.
- (51) Lee, C. H.; Tian, L.; Abbas, A.; Kattumenu, R.; Singamaneni, S. Directed Assembly of Gold Nanorods Using Aligned Electrospun Polymer Nanofibers for Highly Efficient SERS Substrates. *Nanotechnology* **2011**, *22*, 275311.
- (52) Sau, T. K.; Murphy, C. J. Seeded High Yield Synthesis of Short Au Nanorods in Aqueous Solution. *Langmuir* **2004**, *20*, 6414–6420.
- (53) Vigderman, L.; Manna, P.; Zubarev, E. R. Quantitative Replacement of Cetyl Trimethylammonium Bromide by Cationic Thiol Ligands on the Surface of Gold Nanorods and Their Extremely Large Uptake by Cancer Cells. *Angew. Chem., Int. Ed.* **2012**, *51*, 636–641.
- (54) Zubarev, E. R.; Khanal, B. P. Rings of Nanorods. *Angew. Chem., Int. Ed.* **2007**, *46*, 2195–2198.
- (55) Wu, H. Y.; Chu, H. C.; Kuo, T. J.; Kuo, C. L.; Huang, M. H. Seed-Mediated Synthesis of High Aspect Ratio Gold Nanorods with Nitric Acid. *Chem. Mater.* **2005**, *17*, 6447–6451.
- (56) Gole, A.; Murphy, C. J. Seed-Mediated Synthesis of Gold Nanorods: Role of the Size and Nature of the Seed. *Chem. Mater.* **2004**, *16*, 3633–3640.
- (57) Nikoobakht, B.; El-Sayed, M. A. Preparation and Growth Mechanism of Gold Nanorods (NRs) Using Seed-Mediated Growth Method. *Chem. Mater.* **2003**, *15*, 1957–1962.
- (58) Sharma, V.; Park, K.; Srinivasarao, M. Colloidal Dispersion of Gold Nanorods: Historical Background, Optical Properties, Seed-Mediated Synthesis, Shape Separation and Self-Assembly. *Mater. Sci. Eng., R* **2009**, *65*, 1–38.
- (59) Van Der Zande, B. M. I.; Pages, L.; Hikmet, R. A. M.; Van Blaaderen, A. Optical Properties of Aligned Rod-Shaped Gold Particles Dispersed in Poly(Vinyl Alcohol) Films. *J. Phys. Chem. B* **1999**, *103*, 5761–5767.
- (60) Vigderman, L.; Zubarev, E. R. High-Yield Synthesis of Gold Nanorods with Longitudinal SPR Peak Greater Than 1200 nm Using Hydroquinone as a Reducing Agent. *Chem. Mater.* **2013**, *25*, 1450–1457.
- (61) Tian, L. M.; Chen, E.; Gandra, N.; Abbas, A.; Singamaneni, S. Gold Nanorods as Plasmonic Nanotransducers: Distance-Dependent Refractive Index Sensitivity. *Langmuir* **2012**, *28*, 17435–17442.
- (62) Bao, Y.; Luu, Q. A. N.; Zhao, Y.; Fong, H.; May, P. S.; Jiang, C. Upconversion Polymeric Nanofibers Containing Lanthanide-Doped Nanoparticles via Electrospinning. *Nanoscale* **2012**, *4*, 7369–7375.
- (63) Yu, C. X.; Irudayaraj, J. Multiplex Biosensor Using Gold Nanorods. *Anal. Chem.* **2007**, *79*, 572–579.
- (64) Kudo, S.; Otsuka, E.; Suzuki, A. Swelling Behavior of Chemically Crosslinked PVA Gels in Mixed Solvents. *J. Polym. Sci., Part B: Polym. Phys.* **2010**, *48*, 1978–1986.
- (65) Schack, N. B.; Oliveira, C. L. P.; Young, N. W. G.; Pedersen, J. S.; Ogilby, P. R. Oxygen Diffusion in Cross-Linked, Ethanol-Swollen Poly(Vinyl Alcohol) Gels: Counter-Intuitive Results Reflect Microscopic Heterogeneities. *Langmuir* **2009**, *25*, 1148–1153.
- (66) Chang, J. Y.; Godovsky, D. Y.; Han, M. J.; Hassan, C. M.; Kim, J.; Lee, B.; Peppas, N. A.; Quirk, R. P.; Yoo, B. *Biopolymers · PVA Hydrogels Anionic Polymerisation Nanocomposites*; Springer: Berlin, 2000; Vol. 153.